




## RESEARCH PAPER

# Amyloid precursor protein induces reactive astrogliosis

Gretsen Velezmoro Jauregui<sup>1</sup>  | Dragana Vukić<sup>2,3</sup> | Isaac G. Onyango<sup>1</sup> | Carlos Arias<sup>4</sup> | Jan S. Novotný<sup>5</sup> | Kateřina Texlová<sup>1</sup> | Shanshan Wang<sup>6,7</sup> | Kristina Locker Kovačovicova<sup>8</sup> | Natalie Polakova<sup>5</sup> | Jana Zelinkova<sup>5</sup> | Maria Čarna<sup>5</sup> | Valentina Lacovich<sup>2</sup> | Brian P. Head<sup>6,7</sup> | Daniel Havas<sup>8</sup> | Martin Mistrik<sup>5</sup> | Robert Zorec<sup>9,10</sup> | Alexei Verkhratsky<sup>11,12,13,14</sup>  | Liam Keegan<sup>2</sup> | Mary A. O'Connell<sup>2</sup> | Robert Rissman<sup>4</sup> | Gorazd B. Stokin<sup>1,5,15</sup> 

<sup>1</sup>Translational Ageing and Neuroscience Program, Centre for Translational Medicine, International Clinical Research Centre, St. Anne's University Hospital, Brno, Czech Republic

<sup>2</sup>Central European Institute of Technology, Masaryk University, Brno, Czech Republic

<sup>3</sup>Faculty of Science, National Centre for Biomedical Research, Masaryk University, Brno, Czech Republic

<sup>4</sup>Department of Neurosciences, University of California San Diego, La Jolla, California, USA

<sup>5</sup>Faculty of Medicine and Dentistry, Institute of Molecular and Translational Medicine, Palacky University Olomouc, Olomouc, Czech Republic

<sup>6</sup>Veterans Affairs San Diego Healthcare System, San Diego, USA

<sup>7</sup>Department of Anesthesia, University of California San Diego, La Jolla, California, USA

<sup>8</sup>PsychoGenics, Paramus, New Jersey, USA

<sup>9</sup>Laboratory of Neuroendocrinology, Molecular Cell Physiology, Faculty of Medicine, Institute of Pathophysiology, University of Ljubljana, Ljubljana, Slovenia

<sup>10</sup>Celica Biomedical, Technology Park, Ljubljana, Slovenia

<sup>11</sup>Faculty of Biology, Medicine and Health, University of Manchester, Manchester, UK

<sup>12</sup>Achucarro Centre for Neuroscience, IKERBASQUE, Basque Foundation for Science, Bilbao, Spain

<sup>13</sup>Department of Stem Cell Biology, State Research Institute Centre for Innovative Medicine, Vilnius, Lithuania

<sup>14</sup>Department of Forensic Analytical Toxicology, School of Forensic Medicine, China Medical University, Shenyang, Liaoning Province, China

<sup>15</sup>Department of Neurology, Gloucestershire Royal Hospital, Gloucestershire NHS Foundation Trust, Gloucester, UK

## Correspondence

Gorazd B. Stokin, Translational Ageing and Neuroscience Program, Centre for Translational Medicine, International Clinical Research Centre, St. Anne's University Hospital, Brno, Czech Republic.

Email: [gbstokin@alumni.ucsd.edu](mailto:gbstokin@alumni.ucsd.edu)

## Funding information

The European Union: Next Generation EU – Project National Institute for Neurological Research, Grant/Award Number: (EXCELES, LX22NPO5107 (MEYS)) (G.B.S.); The Slovenian Research Agency project, Grant/Award

## Abstract

**Aim:** Astrocytes respond to stressors by acquiring a reactive state characterized by changes in their morphology and function. Molecules underlying reactive astrogliosis, however, remain largely unknown. Given that several studies observed increase in the Amyloid Precursor Protein (APP) in reactive astrocytes, we here test whether APP plays a role in reactive astrogliosis.

**Methods:** We investigated whether APP instigates reactive astrogliosis by examining in vitro and in vivo the morphology and function of naive and APP-deficient astrocytes in response to APP and well-established stressors.

**Results:** Overexpression of APP in cultured astrocytes led to remodeling of the intermediate filament network, enhancement of cytokine production, and

This is an open access article under the terms of the [Creative Commons Attribution-NonCommercial-NoDerivs](https://creativecommons.org/licenses/by-nc-nd/4.0/) License, which permits use and distribution in any medium, provided the original work is properly cited, the use is non-commercial and no modifications or adaptations are made.

© 2024 The Authors. *Acta Physiologica* published by John Wiley & Sons Ltd on behalf of Scandinavian Physiological Society.

Number: J3-50104 (R.Z.); The Czech Science Foundation GAČR, Grant/Award Number: 21-27329X (M.A.O. and L.K.); The Slovenian Research Agency Core Research Program P3 310 Cell Physiology (R.Z.); The European Regional Development MAGNET, Grant/Award Number: CZ.02.1.01/0.0./15\_003/0000492 (G.B.S.); The European Regional Development ENOCH, Grant/Award Number: CZ02.1.01/0.0/16\_019/0000868 (G.B.S.); Interreg ITA-SLO ImmunoCluster-2; CipKeBip (R.Z.); VA Merit Award, Grant/Award Number: 5I01BX003671 (B.P.H.); VA Research Career Scientist Award, Grant/Award Number: 1IK6BX006318 (B.P.H.)

activation of cellular programs centered around the interferon (IFN) pathway, all signs of reactive astrogliosis. Conversely, APP deletion abrogated remodeling of the intermediate filament network and blunted expression of IFN-stimulated gene products in response to lipopolysaccharide. Following traumatic brain injury (TBI), mouse reactive astrocytes also exhibited an association between APP and IFN, while APP deletion curbed the increase in glial fibrillary acidic protein observed canonically in astrocytes in response to TBI.

**Conclusions:** The APP thus represents a candidate molecular inducer and regulator of reactive astrogliosis. This finding has implications for understanding pathophysiology of neurodegenerative and other diseases of the nervous system characterized by reactive astrogliosis and opens potential new therapeutic avenues targeting APP and its pathways to modulate reactive astrogliosis.

#### KEYWORDS

amyloid precursor protein, astrocytes, interferon pathway, lipopolysaccharide, reactive astrogliosis, traumatic brain injury

## 1 | INTRODUCTION

Astrocytes are homeostatic cells of the central nervous system (CNS) that provide support and regulate various aspects of the functional activity of the nervous tissue being fundamental elements of the brain active milieu.<sup>1</sup> In particular, astrocytes contribute to the regulation of synaptic transmission,<sup>2-5</sup> energy metabolism,<sup>6-9</sup> and maintenance of the blood brain barrier.<sup>10-13</sup> Brain lesions trigger reactive astrogliosis which, together with microgliosis and reactive remodeling of oligodendrocyte precursor cells, represents evolutionary conserved defensive response aimed at protection and postlesional restoration of the nervous tissue from various forms of pathological stressors and insults.<sup>14,15</sup> Reactive astrogliosis proceeds through complex, still poorly understood, reorganization of astrocytic biochemistry, morphology, and physiology to create multiple contexts- and disease-specific reactive phenotypes.<sup>16,17</sup> Reactive astrogliosis is linked to the activation of several cellular programs and second messenger signaling pathways<sup>15,18</sup> that await to be fully elucidated.<sup>19-23</sup> In particular, reactive astrocytes up-regulate synthesis and release of pro-inflammatory proteins such as cytokines<sup>24,25</sup> and antigen-presenting molecules.<sup>26</sup> Molecular pathways that trigger and regulate the progression of reactive astrogliosis remain however largely unknown.

Accumulating evidence indicates that various insults instigating reactive astrogliosis increase expression of the amyloid precursor protein (APP), an astrocyte resident type I integral membrane protein involved in many physiological and pathophysiological processes.<sup>27-31</sup> For example, intraperitoneal injection of lipopolysaccharide (LPS),

an archetypal pathogen-associated molecular pattern, increases APP levels in astrocytes in mice and rats.<sup>32-34</sup> Similar increase was observed after intraventricular injection of LPS<sup>35</sup> or by adding LPS to astrocyte culture media.<sup>36</sup> Treatment with cytokines such as interleukin-1 (IL-1),<sup>36-40</sup> tumor necrosis factor  $\beta$  (TNF $\beta$ ),<sup>38,39,41</sup> tumor necrosis factor  $\alpha$  (TNF $\alpha$ )<sup>36</sup> and interferon  $\gamma$  (IFN $\gamma$ )<sup>36,37</sup> increased APP levels in astrocytes both in vitro and in vivo. Astrocytic APP levels increase also in response to many pathological conditions including ischemia,<sup>42</sup> brain trauma<sup>43,44</sup> heat shock,<sup>45</sup> cuprizone-induced demyelination,<sup>46</sup> quinolinic acid excitotoxicity<sup>47</sup> and hyperammonaemia<sup>48,49</sup> as well as following increase in cytoplasmic cyclic adenosine monophosphate (cAMP).<sup>50</sup> In all these conditions, astrocytes generate molecules involved in inflammation including cytokines.<sup>51-53</sup> There is little knowledge, however, of how molecular mechanisms exactly orchestrate the acquisition of this reactive state of astrocytes.

The evidence that all these stressors and conditions do not only induce reactive astrogliosis but invariably increase expression levels of APP in astrocytes led us to hypothesize that APP plays a pivotal role in the transition of astrocytes into a reactive state. To test this hypothesis, we utilized molecular, biochemical, and immunohistochemical approaches in cell culture and in a mouse model of TBI to rigorously investigate the role of 770 amino acid-long APP<sup>31,38</sup> in the initiation of reactive astrogliosis. We found that overexpression of this APP isoform in astrocytes promotes, while deletion of APP abrogates reactive astrogliosis, thus indicating that APP represents a potential molecular switch initiating reactive astrogliosis. Astrocytic APP may thus be a valuable target in the regulation of the response of astroglia to pathological conditions.

## 2 | RESULTS

### 2.1 | APP triggers reactive astrocyte morphology

As alluded before, previous studies showed that stressors inducing reactive astrogliosis at the same time also increase APP expression.<sup>34–36</sup> This raised the question of whether increased APP levels induce reactive state of the astrocytes in the absence of stressors. As the first step, we reproduced previously reported effects of LPS on the GFAP-immunoreactivity and APP levels in the astrocytes<sup>36,40,54</sup> using primary human cortical astrocytes as the experimental model. Cultures were treated with 2 µg/mL LPS for 48 h and GFAP-positive astrocytic profiles were analyzed by the end of this period with the Sholl analysis, determining the number of cell processes, the sum of intersections of processes with concentric circles, the ramification indices, and the ending cell radii (Figures 1A,B and S1). Treatment with LPS increased morphological complexity of astrocytes as evidenced by a significantly increased average number of processes, the sum of intersections, and in the number of intersections versus distance from the soma in comparison to untreated control (Figures 1C and S2). In addition, LPS-treated astrocytes had significantly increased cellular levels of full-length APP whereas there was no change in the ratio of the average mature (fully post-translationally processed) versus immature APP levels compared with untreated astrocytes (Figure 1D).

As the next step, we investigated whether overexpression of the 770 amino acid long APP (APP770-pcDNA3.1) alone induces astrocyte remodeling in the absence of stressors. Transfection of astrocytes with APP770-pcDNA3.1 resulted in a roughly threefold increase in the average levels of cellular APP, with no impact on the mature versus immature APP ratio compared to astrocytes transfected with the pcDNA3.1 empty vector (Figures 1E and S3). As with LPS induction, Sholl analysis revealed that sole overexpression of APP was accompanied by a significant increase in the number of processes, sum of intersections, mean intersections, and in the number of intersections versus distance from the soma of GFAP-positive astrocytes (Figures 1F–H and S4).

Hence a canonical instigator of reactive astrogliosis (LPS) and overexpression of APP both result in the remodeling of the intermediate filament network. This signifies that increased APP levels are sufficient on their own to induce morphological features characteristic of reactive astrocytes. However, the characteristics of astrocytes are very diverse and complex and morphological changes alone are insufficient to conclude on their acquisition of a pathologically relevant reactive state. Thus, we examined

next whether these morphological changes are accompanied by typical functional changes characteristic of reactive astrocytes.

### 2.2 | APP induces the generation of cytokines and activates interferon pathways

To validate an experimental paradigm to track functional changes of the astrocytes, we exposed primary human cortical astrocytes for 48 h to LPS and then measured cytokines using a well-established ELISArray (Figure 2A). In accordance with previous reports,<sup>32,33,35</sup> LPS increased cytokine levels in astrocytes. In particular, LPS led to significant increases in the levels of IFN $\gamma$ , interleukin-6 (IL-6), TNF $\alpha$ , granulocyte colony-stimulating factor (G-CSF), and interleukin-12 (IL-12), and a significant decrease in TGF $\beta$  levels compared with unstimulated astrocytes.

We next measured cytokine levels in primary human cortical astrocytes transfected with pcDNA3.1 (empty vector), CMV, and GFP-pcDNA3.1 as controls or with APP770-pcDNA3.1 (Figure 2B). Transfection of astrocytes with APP770-pcDNA3.1 resulted in a significant increase in IFN $\gamma$ , G-CSF, interleukin-5 (IL-5), interleukin-10 (IL-10), IL-12, interleukin 13 (IL-13) and a significant decrease in IL-6, interleukin-4 (IL-4) and TGF $\beta$ 1 levels compared with astrocytes transfected with pcDNA3.1. Transfection of astrocytes with CMV empty vector or GFP-pcDNA3.1 produced significant changes in IL-6 and IL-13 levels compared with pcDNA3.1 only. This indicates a marginal effect of empty vector or generally foreign protein on the cytokine expression and DNA sensing pathways.<sup>55</sup> In contrast to LPS treatment, overexpression of APP produced significant changes in astrocytic levels of TGF $\beta$ 1, IL-5, IL-10, and IL-6 (Figure 2C). The results of these experiments indicate that APP overexpression induces cytokine production in astrocytes with cytokine changes mediated by APP exhibiting a unique cytokine profile that differs from the one obtained following LPS treatment.

To test whether the observed changes in cellular cytokine levels following APP overexpression are reflected in enhanced gene expression and to identify the most significantly activated cellular programs, astrocytes transfected with either pcDNA3.1 empty vector or APP770-pcDNA3.1 were sequenced for their RNA. Heatmap and principal component analysis showed significant differences in the transcriptional profiles in the APP770-pcDNA3.1 compared with the pcDNA3.1 transfected astrocytes (Figure 2D,E). Volcano plots identified several significantly upregulated and no downregulated differentially expressed genes in the APP770-pcDNA3.1 compared with the pcDNA3.1 transfected astrocytes (Figure 2F).

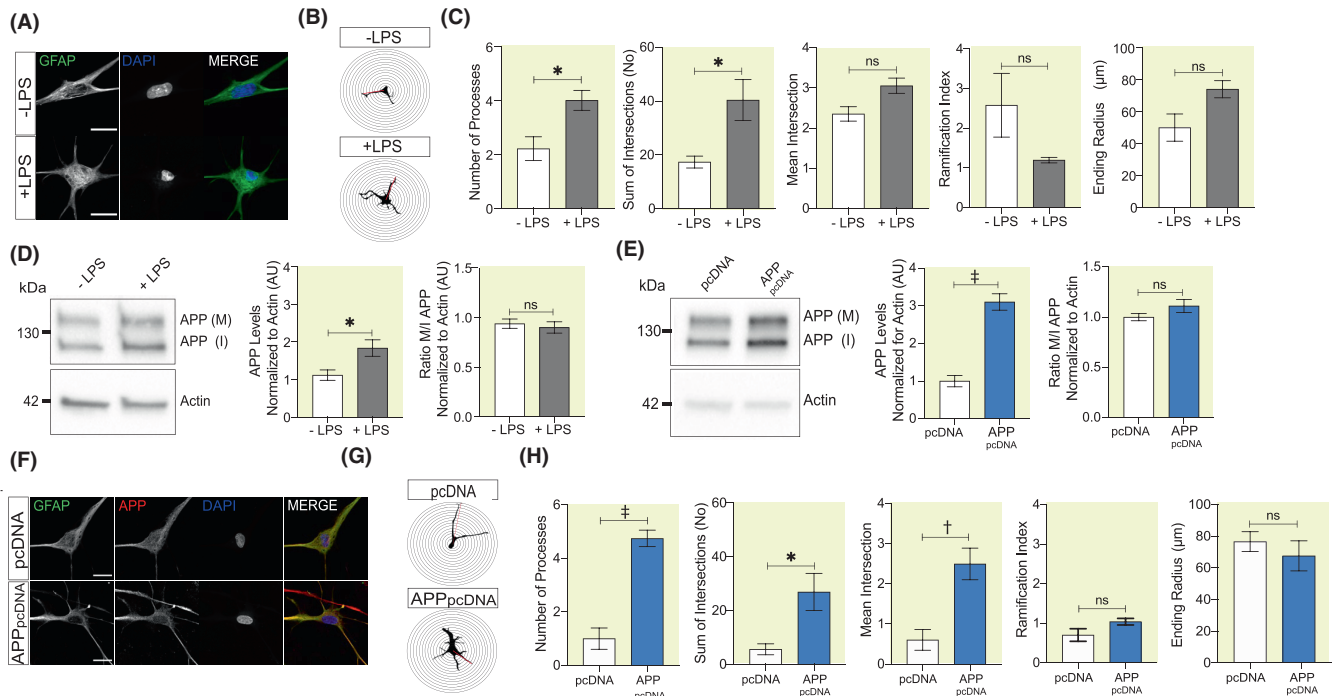


**FIGURE 1** APP promotes remodeling of GFAP-positive astrocytic profiles. (A) Representative images of untreated (–LPS) and LPS-treated (+LPS) primary human cortical astrocytes stained with GFAP and DAPI (Scale bar 20 μm). (B) Representative image reconstructions of –LPS and +LPS GFAP-stained astrocytes based on the Sholl analysis using 5 μm spacing between the concentric circles. (C) Comparison of key Sholl analysis parameters between –LPS and +LPS GFAP-stained astrocytes (5 to 8 cells were analyzed per condition per experiment, each experiment was performed 3 times, *t*-test, \**p* < 0.05). (D) Representative blot showing APP levels in –LPS and +LPS astrocytes normalized for actin levels as a loading control. Graphs show mean levels of APP normalized for actin (left) and the mean ratio between mature (M) versus immature (I) APP (right) (*N* = 5 biological samples per condition, *t*-test, \**p* < 0.05). (E) Representative blot showing APP levels in astrocytes transfected with either pcDNA3.1 (pcDNA) or APP770-pcDNA3.1 (APPpcDNA) normalized for actin levels as a loading control. Graphs show average mean levels of APP normalized for actin (left) and the mean ratio of mature (M) versus immature (I) APP (right) (*N* = 5 biological samples per condition, *t*-test, ns = not significant). (F) Representative images of astrocytes transfected with either pcDNA3.1 (pcDNA) or APP770-pcDNA3.1 (APPpcDNA) and stained with GFAP, APP, and DAPI (Scale bar 20 μm). (G) Representative image reconstructions of GFAP-stained astrocytes transfected with either pcDNA3.1 (pcDNA) or APP770-pcDNA3.1 (APPpcDNA) based on the Sholl analysis using 5 μm spacing between the concentric circles. (H) Comparison of key Sholl morphometric analysis of GFAP-stained astrocytes transfected either with pcDNA3.1 or with APP770-pcDNA3.1 (three to five cells were analyzed per condition per experiment, each experiment was performed four times, *t*-test, \**p* < 0.05, †*p* < 0.01, ‡*p* < 0.001).

Gene ontology enrichment analysis showed that overexpression of APP mostly upregulated interferon, cytokine, and inflammasome signaling (Figure 2G). Indeed, overexpression of APP led to significantly increased astrocyte IFN $\gamma$  and IFN $\beta$  at the transcriptional and protein level (Figures 2G and S5). Comparison of the transcriptomic profiles between astrocytes transfected with either APP770-pcDNA3.1 or APP770-pcDNA3.1 carrying the familial Swedish, Florida, Austrian, Arctic or Icelandic APP mutation<sup>56–60</sup> showed no differences between profiles, indicating that activation of interferon, cytokine, and inflammasome signaling pathways most likely depends on the levels of full-length APP rather than on the mutation-induced changes in its proteolytic processing (Figure S6). These results indicate that overexpression of APP induces not only morphological but also functional features of reactive astrocytes.

### 2.3 | Increased APP- and IFN $\gamma$ -immunoreactivity in reactive astrocytes following TBI

To test for the physiological relevance of the observed relationship between APP and the cytokines in primary human cortical astrocytes, we studied APP- and IFN $\gamma$  in reactive astrocytes following controlled cortical impact (CCI), a well-established mouse model of traumatic brain injury (TBI) (Figure 3A).<sup>61</sup> We first examined the morphology of GFAP-stained astrocytes in the corpus callosum in an area positioned just under the CCI region using the Sholl analysis (Figure 3B,C). Two months following CCI, GFAP-immunoreactive astrocytes exhibited significantly increased numbers of processes, and more intersections and mean intersections in TBI compared with control mice (Figure 3D). As previously reported,<sup>62</sup>



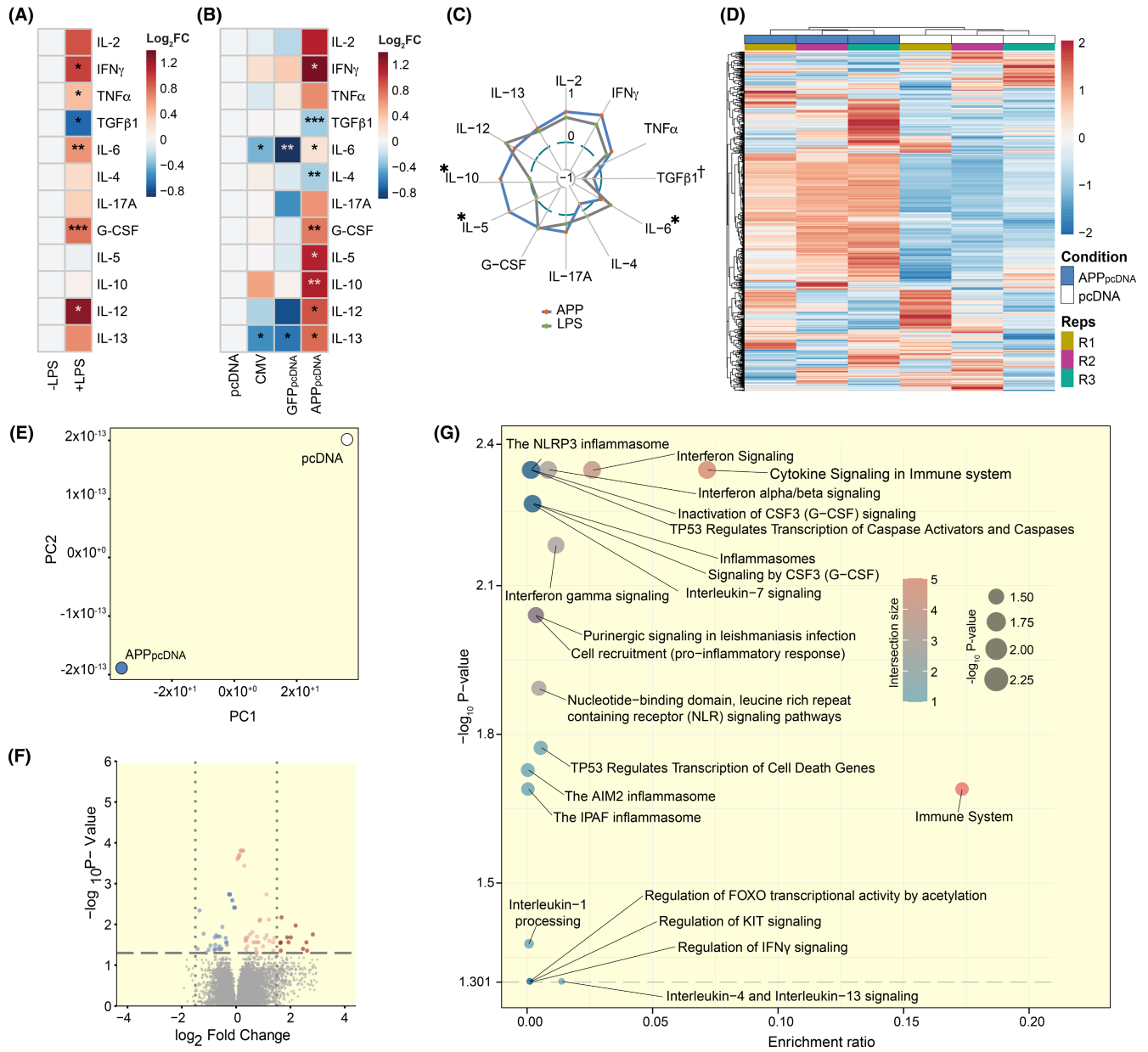
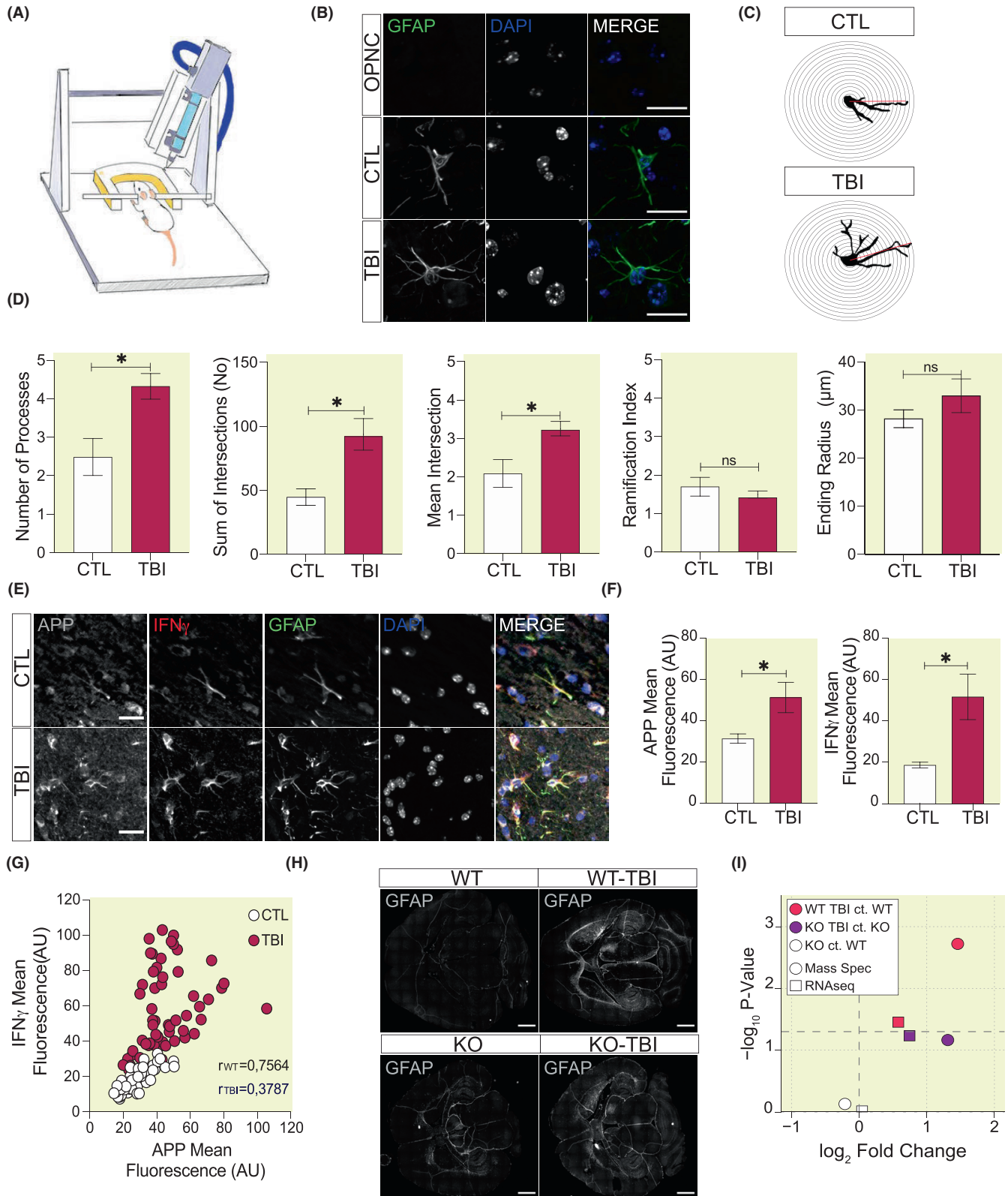


**FIGURE 2** APP increases the expression of cytokines in astrocytes. (A) Heatmap showing changes in abundances of cytokines in -LPS and +LPS astrocytes ( $N = 3$  biological samples per condition,  $t$ -test, \* $p < 0.05$ , † $p < 0.01$ , ‡ $p < 0.001$ ). Individual protein concentrations (pg/mg) were  $\log_2$  transformed. (B) Heatmap showing changes in abundances of cytokines in pcDNA3.1 (pcDNA), CMV, GFP-pcDNA3.1 (GFPpcDNA) and APP770-pcDNA3.1 (APPpcDNA) transfected astrocytes ( $N = 3$  biological samples per condition,  $t$ -test, \* $p < 0.05$ , † $p < 0.01$ , ‡ $p < 0.001$ ). Individual protein concentrations (pg/mg) were  $\log_2$  transformed. (C) Radar plot showing changes in cytokine profiles between LPS treated and APP770-pcDNA3.1 transfected astrocytes ( $N = 3$  biological samples per condition, ANOVA with Tukey post-hoc test, \* $p < 0.05$ , † $p < 0.01$ ). (D) Bidirectionally clustered heatmap showing the expression of 1000 genes with the highest variability. Color annotations differentiate individual astrocyte treatments and replicates. (E) Principal Component Analysis (PCA) of transcriptomic profiles of APP770-pcDNA3.1 versus pcDNA3.1 empty vector-transfected astrocytes. (F) Volcano plot showing differentially expressed (DE) genes in astrocytes transfected with APP770-pcDNA3.1 and pcDNA3.1. The horizontal line indicates statistically significant DE genes, vertical dotted lines indicate the  $\log_2$  FC of  $\pm 1.5$ . (G) The most significantly changed REACTOME pathways by the DE genes with  $\log_2$  FC exceeding the cut-off of  $\pm 1.5$ .

TBI triggered reactive astrogliosis, which led us next to investigate the relationship between APP- and IFN $\gamma$ -immunoreactivities in reactive astrocytes following TBI. After a series of pilot experiments to optimize labeling and

imaging (Figure S7), we found that GFAP-stained reactive astrocytes showed significantly increased APP- and IFN $\gamma$ -immunoreactivities in TBI compared with sham-operated mice (Figure 3E,F). In addition, a significant positive



correlation was observed between the mean intensities of APP- and IFN $\gamma$ -immunoreactive signals in astrocytes in control and TBI mice (Figure 3G). These exploratory experiments corroborate in vivo functional association between APP and IFN $\gamma$  previously found in cell culture by identifying a direct relationship between APP- and

IFN $\gamma$ -immunoreactivities in reactive astrocytes following TBI.

Finally, we examined whether APP contributes to the increase in GFAP content in astrocytes after TBI in vivo (Figures 3H,I and S8). To this end, we analyzed GFAP expression and levels in wildtype mice (WT), WT mice

**FIGURE 3** APP and IFN $\gamma$  in astrocytes following TBI. (A) Cartoon depicting the controlled cortical impact (CCI) injury model of the traumatic brain injury (TBI). (B) Representative confocal microscopy images of OPNC (omitted primary negative control) and GFAP-stained astrocytes in the corpus callosum of control and TBI mice (scale bar 20  $\mu$ m). (C) Representative reconstructed images of GFAP-immunoreactive astrocytes of the corpus callosum of control and TBI mice based on the Sholl analysis with a 5  $\mu$ m interval of the concentric circles. (D) Measurements of key Sholl parameters in GFAP-stained astrocytes in control and TBI mice (five to seven per animal,  $N=4$  mice,  $t$ -test,  $*p < 0.05$ ). (E) Representative confocal microscopy images of APP- and IFN $\gamma$ -immunoreactivities in GFAP-stained astrocytes in corpus callosum of control and TBI mice (Scale bar 20  $\mu$ m). (F) Graph showing mean APP- and IFN $\gamma$ -immunoreactivities in GFAP-stained astrocytes in the corpus callosum of control and TBI mice ( $N=4$  mice,  $t$ -test,  $*p < 0.05$ ). (G) Relationship between mean APP- and IFN $\gamma$ -immunoreactivities in the GFAP-stained astrocytes in the corpus callosum of control and TBI mice ( $N=4$  mice, Pearson correlation coefficient ANOVA two-tailed  $\dagger p < 0.01$ ,  $\ddagger p < 0.001$ ). (H) Representative GFAP-stained brain sections from wildtype (WT) and APP knock-out (KO) mice subject or not to traumatic brain injury (TBI). (I) Differentially expressed genes and protein levels of GFAP content in brains from wildtype (WT) and APP knock-out (KO) mice subject or not to traumatic brain injury (TBI). The horizontal line indicates statistically significant differences ( $N=3$  mice).

following CCI (WT TBI), APP knock out mice (KO) and KO mice following TBI (KO TBI) obtained from an ongoing RNA-Seq and tandem mass tag mass spectrometry (TMT-MS) study. Compared with brains from WT mice, GFAP mRNA expression and protein levels in WT TBI mice were significantly increased ( $N=3$ ; 0.58-fold ( $p=0.035$ ) and 1.45-fold ( $p=0.002$ )) as revealed by RNA-Seq and TMT-MS, respectively (Figure 3H). In contrast, there were no significant differences in GFAP levels, determined by RNA-Seq or TMT-MS when comparing KO TBI with KO ( $N=3$ ;  $p_{\text{RNA-Seq}}=0.059$ ,  $p_{\text{TMT-MS}}=0.069$ ) or KO to WT ( $N=3$ ;  $p_{\text{RNA-Seq}}=0.938$ ,  $p_{\text{TMT-MS}}=0.744$ ). These preliminary findings align with our previous observations in cell culture, indicating an *in vivo* connection between APP- and IFN $\gamma$ -immunoreactivities in reactive astrocytes following TBI and underscore the putatively crucial role of APP in triggering reactive astrogliosis.

## 2.4 | LPS-induced reactive astrogliosis requires APP

Our findings suggest that APP induces morphological and functional features characteristic of reactive astrocytes in cell culture as well as in the *in vivo* brain. These experiments, however, do not critically test whether APP is required for reactive remodeling of astrocytes. To test this hypothesis, we deleted APP in astrocytes, treated cultures with LPS, and subsequently analyzed morphology of GFAP-positive astrocytic profiles and measured levels of a panel of IFN-stimulated gene (ISG) products. To confirm the impact of LPS treatment and the deletion of APP induced by the multiMIR-APP lentiviral vector, we initially measured cellular APP levels normalized to actin using western blots (Figure 4A). This analysis revealed a significant increase and decrease in APP levels in astrocytes subjected to LPS treatment or transduced with the multiMIR-APP lentiviral vector, respectively. Whether we used a multiMIR-APP vector or a control

vector (multiMIR-Scramble), Sholl analysis of GFAP-labeled primary human cortical astrocytes (Figure 4B,C) demonstrated similar cell morphologies. Consistent with our previous findings, LPS-treated astrocytes displayed a notable increase in the mean number of processes compared to untreated astrocytes (Figure 4D). Deletion of APP using the multiMIR-APP lentiviral vector nullified the LPS-induced increase in the mean number of processes in astrocytes. Consequently, astrocytes lacking APP appear unable to mount a reactive response to LPS.

We next measured cellular levels of a panel of ISG products including adenosine deaminase acting on RNA p110 (ADAR1p110), adenosine deaminase acting on RNA p150 (ADAR1p150), protein kinase R (PKR), melanoma differentiation-associated protein 5 (MDA-5) and retinoic acid-inducible gene 1 (RIG-1) all normalized to GAPDH (Figure 4E). To examine changes in the levels of cellular ISG products following APP deletion and LPS treatment, we measured either their expression ratios or log<sub>2</sub> fold changes, first between astrocytes transduced with multiMIR-APP versus multiMIR-Scramble, and then between LPS-treated astrocytes transduced with multiMIR-APP versus multiMIR-scramble lentiviral vectors. We observed significant reduction in ADAR1p110- and PKR-ratio and significant log<sub>2</sub> fold change of both ADAR1 isoforms between multiMIR-APP and multiMIR-Scramble transduced astrocytes (Figure 4F). Comparing cellular ISG product levels between LPS-treated multiMIR-APP- and multiMIR-Scramble-transduced astrocytes, we observed significant reductions in MDA5, PKR, and ADAR1p110 ratios and MDA5, RIG-1, PKR and both ADAR1 isoforms log<sub>2</sub> fold changes (Figure 4G). The results of these measurements indicated that APP deletion alone is sufficient to perturb levels of ISG products in naïve astrocytes and prevent their increase in response to LPS. Collectively, these data suggest that APP deletion suppresses reactive astrogliosis.

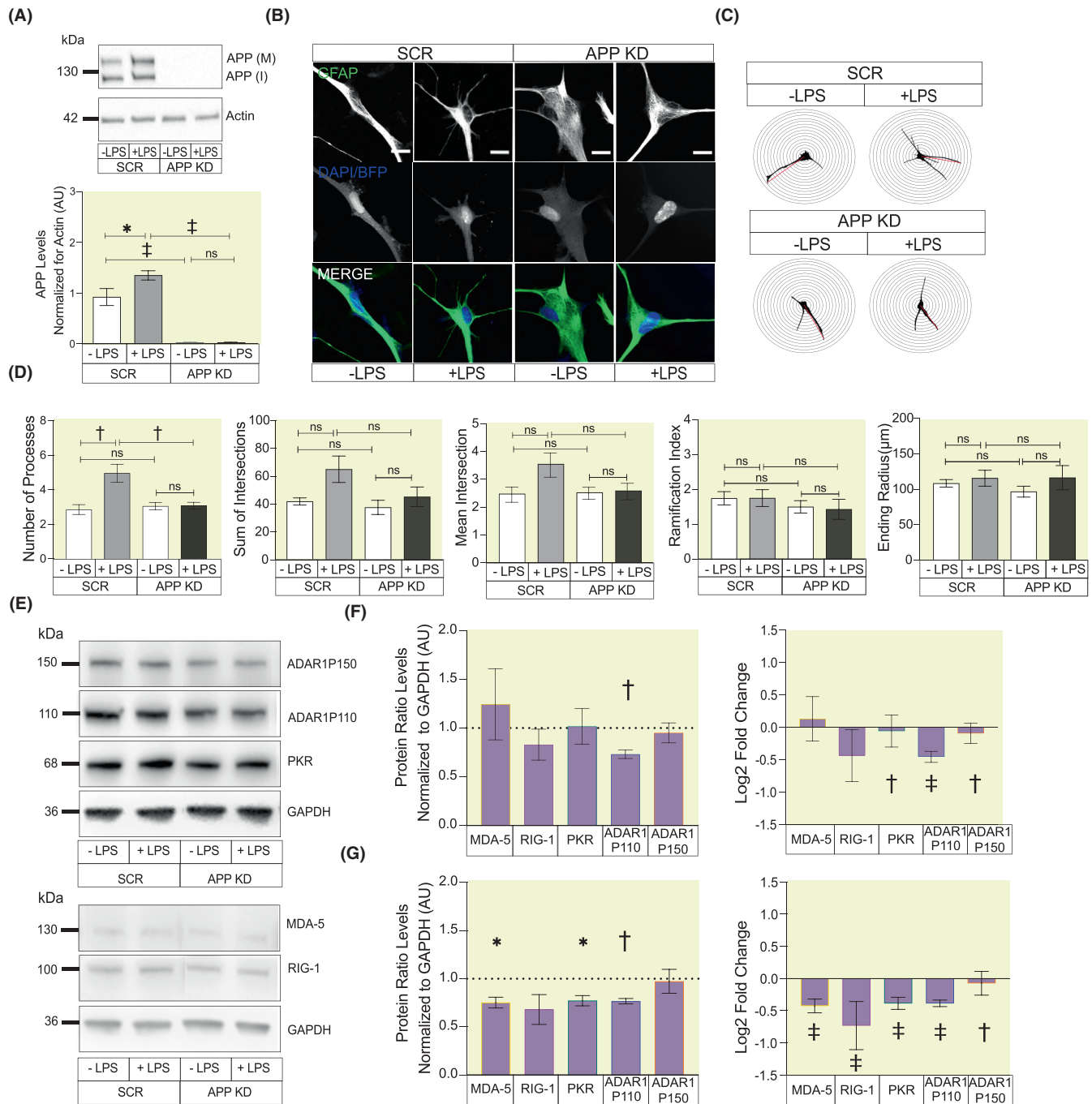


**FIGURE 4** Deletion of APP hampers reactive astrogliosis in response to LPS. (A) Representative western blot showing levels of APP normalized for actin as a loading control in untreated (–LPS) and LPS treated (+LPS) astrocytes transduced with multiMIR-Scramble (SCR) and multiMIR-APP (APP KD) lentiviral vectors. Graph showing mean APP levels normalized for actin ( $N = 5$  biological replicates, ANOVA with Tukey's multiple comparisons test, ns = not significant, \* $p < 0.05$ , † $p < 0.01$ , ‡ $p < 0.001$ ). (B) Representative confocal microscopy images of GFAP-stained –LPS and +LPS astrocytes transduced with multiMIR-Scramble and multiMIR-APP lentiviral vectors (Scale bar 20  $\mu\text{m}$ ). (C) Representative reconstructed images of GFAP-stained –LPS and +LPS astrocytes transduced with multiMIR-Scramble and multiMIR-APP lentiviral vectors based on the Sholl analysis with a 5  $\mu\text{m}$  interval of the concentric circles. (D) Measurements of key Sholl parameters in GFAP-immunoreactive –LPS and +LPS astrocytes transduced with multiMIR-Scramble and multiMIR-APP lentiviral vectors (10 to 27 cells per treatment,  $N = 4$  biological replicates/mice, ANOVA with Tukey's multiple comparisons test, † $p < 0.01$ ). (E) Representative western blot of ISG product levels and GAPDH levels as a loading control in –LPS and +LPS astrocytes transduced with multiMIR-Scramble and multiMIR-APP lentiviral vectors. (F) Graph showing ratios of GAPDH normalized cellular ISG product levels (left, One Sample  $t$ -test, \* $p < 0.05$ , † $p < 0.01$ ) and their geometrical differences presented as log<sub>2</sub> fold changes (right,  $t$ -test with Benjamin–Hochberg correction, † $p < 0.01$ , ‡ $p < 0.001$ ) between multiMIR-Scramble and multiMIR-APP transduced astrocytes ( $N = 4$  biological replicates). (G) Graph showing ratios of GAPDH normalized cellular ISG product levels (left, One Sample  $t$ -test, \* $p < 0.05$ , † $p < 0.01$ ) and their geometrical differences presented as log<sub>2</sub> fold changes (right,  $t$ -test with Benjamin–Hochberg correction, \* $p < 0.05$ , † $p < 0.01$ , ‡ $p < 0.001$ , between –LPS and +LPS multiMIR-Scramble and multiMIR-APP transduced astrocytes ( $N = 4$  biological replicates).



### 3 | DISCUSSION

Increased APP levels in reactive astrocytes were widely reported,<sup>32,36,37,39,40,63</sup> but the underlying rationale for increased APP levels in reactive astrocytes remained so far largely veiled. We here demonstrate that increased expression of APP translates into remodeling of GFAP-positive astrocytic morphology profiles reflecting changes in intermediate filament network, increased production of cytokines, and activation of the IFN pathways. An increase in APP alone is therefore sufficient to induce reactive astrogliosis. Conversely, depletion of APP abrogates LPS-induced reactive astrogliosis and reduces expression of ISG products. To examine whether our findings apply to realistic pathological contexts, we preliminarily build upon previous work in animal models of brain trauma.<sup>22,64–67</sup> These previous studies, however, did not show the interaction between APP and IFN in reactive astrocytes revealed by the present study. In the attempt to translate our cell culture findings into pathophysiologically relevant animal models, we explored and observed an association between APP and IFN levels in reactive astrocytes affected by TBI.<sup>61</sup> This early work of ours supports the idea that APP might well be a key player in triggering and regulating reactive astrogliosis. Thus, we here identify APP as a potential molecular inducer and regulator of reactive astrogliosis.

Understanding this putative role of APP in instigating reactive astrogliosis requires further validation and mechanistic studies, perhaps by taking advantage of human stem cell-derived astrocyte cell lines<sup>68–70</sup> in addition to astrocyte-centered APP overexpressing or deficient animal models and human post-mortem brains.<sup>71,72</sup> Although we performed LPS titration studies prior to starting the proper experimental work, using different concentrations of LPS dissolved in different solvents would be of benefit. Longitudinal study assessing the response of astrocytes to LPS at different time points would also be informative. Different positive controls such as using different astroglial stimulants would be likewise of benefit and in our hands, IL-1 behaved largely comparably to LPS (data not shown). Although we used several constructs as controls for the possible confounding effect of the DNA sensing pathways, including untreated astrocytes or mock-transfected astrocytes in our experimental design would also be valuable. Among the technical caveats, using different methods to demonstrate the same finding is always appreciated. Importantly, the approaches used to analyze data collected from the experiments are always subject to scrutiny. For example, Sholl analysis was designed to study dendritic arborisation,<sup>73</sup> and considering it involves manual tracing it's always at least to some extent subjective. Equally so, the thresholds used for RNA sequencing

are also subject to a rather arbitrary definition. Favorably, despite all of these possible pitfalls, our efforts to perform experiments rigorously produced results that are largely aligned with previous work about APP in astrocytes.<sup>37,39,44</sup>

Lack of changes in the transcriptomic profiles of astrocytes transfected with wildtype or familial APP mutations corroborates previous reports indicating that proteolytic processing of APP differs between astrocytes and neurons<sup>74–78</sup> and suggests that full-length APP rather than its proteolytic fragments instigate reactive astrogliosis. Whether this is related to the dominance of the Ox-2 immunoglobulin- and Kunitz-type protease inhibitor domains-containing 770 amino acid long APP isoform,<sup>31,38,79–81</sup> which is enriched in astrocytes in AD,<sup>82,83</sup> remains to be investigated. A wealth of data documents that exposure to A $\beta$  alone induces reactive astrogliosis<sup>84,85</sup> and activates IFN and other pro-inflammatory pathways.<sup>86</sup> Since at least some of the morphological and functional features characteristic of reactive astrocytes can be triggered by A $\beta$ ,<sup>87–89</sup> these data indicate that APP and its proteolytic fragments, such as A $\beta$ , may regulate the structure and function of the astrocytes in an independent as well as in complementary ways. Since APP and its A $\beta$  fragment have both been demonstrated to induce IFN signaling pathways,<sup>86</sup> which also regulate expression and proteolytic processing of APP including generation of A $\beta$ ,<sup>90,91</sup> these studies suggest a putative positive feedback or a feed-forward loop between APP, its proteolytic fragments and the IFN pathways.<sup>54,92,93</sup> It is therefore plausible to hypothesize that such a feedback loop plays a role in IFN-induced remodeling of the intermediate filament network in the reactive astrocytes.<sup>94–99</sup> Emerging data showing that APP binds to and modifies regulators of cytokine expression,<sup>100–103</sup> together with reportedly blunted innate immune response observed in mice deficient in APP,<sup>104</sup> also suggest that consequences of the interplay between APP and the immune networks might be significantly more far-reaching than previously thought.<sup>105</sup>

### 4 | CONCLUSIONS

Our experiments reveal the role of APP as a potential instigator of reactive astrogliosis. By manipulating APP expression, we observed changes in astrocyte morphology and function, implicating APP as a molecular regulator of reactive astrogliosis. This early work enhances our knowledge about the intricate relationship between APP and astrocytic reactivity with extensive implications in furthering our understanding of brain pathologies and developing novel therapies against neuroinflammatory diseases. Given the accumulating evidence that reactive astrocytes are neuroprotective,<sup>15,106,107</sup> our experiments

also strengthen previously proposed neuroprotective roles of APP across different CNS cell types.<sup>108,109</sup> Without doubt, experiments here presented suggest that astroglial APP plays a key role in the neural tissue response to damage. In prospect, our findings merit being explored in genetic, demyelinating, and other brain disorders that involve reactive astrogliosis.<sup>110–112</sup>

## 5 | MATERIALS AND METHODS

### 5.1 | Cell cultures

Human primary cortical astrocytes (HA, #1800, ScienCell) were grown according to the manufacturer's instructions with two modifications. Astrocyte medium (#1801, ScienCell) was not supplemented with fetal bovine serum (FBS) and the poly-L-lysine was replaced with the matrigel matrix (#356231, Corning). HA were cultured at 37°C and 5% CO<sub>2</sub>. To ensure reproducibility, all experiments were performed with HA at passage number 5. Whenever experiments required treatment with a stressor, the astrocytes were incubated with 2 µg/mL of bacterial endotoxin LPS (LPS-EB, Invitrogen) for 48 h.

### 5.2 | Transfection

HA at 70% confluency were transiently transfected using Lipofectamine 2000 following the manufacturer's instructions (#12566-014, Thermo Fisher). The construct consisting of human APP770 cDNA in the pcDNA3.1 backbone was custom made (*GenScript*, Piscataway) and then sequenced. The plasmid was transfected into HA in a 1:2 DNA to Lipofectamine 2000 ratio. HA were lysed or fixed 48 h later.

### 5.3 | Transduction

To knock-down APP, HA were transduced with a lentivector expressing a multi-miRNA system linked to a blue-fluorescent reporter protein (Flashtherapeutics, Toulouse), which carried either a multiplex of 6 miRNAs targeting APP (multiMIR-APP, pV.2.3.2029) or scramble sequences of the siRNAs targeting APP sequences (multiMIR-Scramble, pV.2.3.2028). The multiMIR-Scramble and multiMIR-APP lentiviral vectors were transduced into astrocytes using 5, 10, or 20 multiplicity of infection (MOI). Five days after transduction, the cells were lysed, and APP levels were measured by western blot. MOI 10 was selected for the experiments as it showed no APP signal compared with APP levels measured in

astrocytes transduced with the multiMIR-Scramble lentiviral vector.

### 5.4 | Animal models

A 3-month-old male wildtype (C57Bl/6) and complete APP knock-out (KO) mice (B6.129S7-*App*<sup>tm1Dbo</sup>/J backcrossed to C57BL/6, Jackson Laboratories, Bar Harbor)<sup>113</sup> were subject either to sham surgery or controlled cortical impact (CCI) using a well-established protocol.<sup>61</sup> All mice were euthanized by rapid decapitation and brains were collected for the analyses. All animal use protocols were approved by the Veterans Administration San Diego Healthcare System Institutional Animal Care and Use Committee (San Diego, USA). Mice were handled in compliance with the Guide for the Care and Use of Laboratory Animals (National Academy of Science, Washington, DC).

### 5.5 | Tissue sampling

Sham-operated and CCI exposed wildtype mouse brains were fixed in 4% PFA, embedded in tissue freezing medium (OCT, #14020108926, Leica Biosystems), and snap-frozen using cooled isopentane. Frozen samples were stored at –80°C until sectioning. Fixed brains were later cut horizontally at 10-micron thickness using a Leica CM1950 cryotome.

### 5.6 | Western blotting

Cells were washed with cold phosphate-buffered saline (PBS), scraped off the plates, and lysed on ice for 30 min with 1X RIPA buffer (#20-188, Merck) supplemented with phosphatase (#P5726, Merck) and proteinase inhibitors (#P8340, Merck). The lysates were then span down (20 min, at 4°C, 14,000 RPM), and protein concentration of collected supernatants was measured using the Pierce BCA Protein Assay Kit (#23227, Thermo Scientific). The samples adjusted to contain equal amounts of protein (10 µg or 12 µg) were next denatured (5 min at 95°C) in loading buffer (#1610747, BioRad) and run on 10% TGX (#4561034, BioRad) or mPAGE 4%–12% Bis-Tris Precast gels (#MP41G10, Merck). Separated proteins were then transferred to PVDF or Nitrocellulose membranes according to the manufacturer's instructions (Bio-Rad, Hercules). After 1 h of blocking in 5% (w/v) BSA (bovine serum albumin) dissolved in TBS-T (20 mmol/L Tris, pH 7.4, 65 mmol/L NaCl, 0.1% Tween 20), the membranes were probed with primary antibodies against APP (1:1000, #ab32136, Abcam), β-actin diluted (1:2000, #A2228, Sigma), ADAR1 diluted (1:3000,

#ABIN2855100, Antibodies-online), RIG-1 diluted (1:1000, #3743, Cell signaling), MDA5 diluted (1:800, #5321, Cell Signalling), PKR diluted (1:2000, #ab184257, Abcam) and GAPDH diluted (1:50000, #60004-1-Ig, Proteintech), washed in TBS-T and incubated with horseradish peroxidase-conjugated anti-rabbit (1:2000, #7074P2, Cell Signalling or 1:80000, #A0545, Merck) and anti-mouse (1:2000, #7076P2, Cell Signalling or 1:5000, #331430, Thermo Fisher) secondary antibodies. The blots were developed using ECL (BioRad, Clarity, 1705060), and captured bands were analyzed using Chemidoc (BioRad, Hercules) and ImageJ.<sup>114</sup>

## 5.7 | ELISA

Cell lysates were homogenized with 1X RIPA on ice for 30 min and then centrifuged for 20 min at 14000 g at 4°C. Cytokines were measured using a multi-analyte ELISA array according to the manufacturer's instructions (#MEH-003A, Qiagen). The INF- $\beta$  and INF- $\gamma$  were measured using single target ELISAs (#DIF50C and #DY814-05, R&D Systems).

## 5.8 | Immunocytochemistry

HA were cultured on coverslips, washed with PBS, fixed with 4% PFA in PBS for 30 min at RT, washed with PBS, and then incubated with the blocking solution (10% goat serum, 0.1% Triton X-100 in PBS) for 1 h at RT. Cultures were then stained overnight at 4°C with primary antibodies against GFAP (1:500, #Z0334, Dako) and APP (1:500, #MAB348, Sigma) dissolved in antibody solution (0.1% Triton X-100 in PBS). Cells were thereafter washed with PBS and stained with secondary antibodies (#A-21206 and #A-31570, Life Technologies) for 1 h at RT. Cells were then washed, stained with DAPI, and mounted on slides with Mowiol. Stained cells were examined with an LSM confocal microscope (LSM780, Zeiss) using a 40x oil-immersion objective. Images were acquired and processed using the ImageJ software.<sup>114</sup>

## 5.9 | Immunohistochemistry

Mouse brain sections were blocked with MOM solution (#MKB-2213, Vector Labs) and then incubated overnight with primary antibodies against INF $\gamma$  (1:100, #MCA1301, Bio-Rad), GFAP (1:1000, #ab53554, Abcam) and APP (1:200, #ab2072, Abcam) or against A $\beta$  (MOAB-2 1:1000, #ab126649, Abcam). The next day, the sections were incubated with donkey anti-mouse (AF555, 1:500, #A31570,

Thermo Fisher), donkey anti-goat (AF488, 1:500, #A11055, Thermo Fisher) and donkey anti-rabbit (AF647, 1:500, #A31573, Thermo Fisher) or donkey anti-mouse (AF555, 1:500, #ab150106, Abcam) secondary antibodies followed by DAPI staining and Mowiol mounting.

Sections stained with secondary antibodies only were used as negative controls. Additionally, bleed through control stainings were incubated with all three primary antibodies and one secondary separately. Stained mouse brain sections were imaged using a 10x objective on AxioScan. Z1 slide scanner microscope (Zeiss, Oberkochen). To better visualize the distribution of specific markers the slides were imaged also with a 63x oil-immersion objective on an LSM780 confocal microscope (Zeiss, Oberkochen).

## 5.10 | Protein extraction and quantification

Brain tissue was weighed and homogenized in lysis buffer (RIPA 1X Millipore, 20-188, 10  $\mu$ L of buffer per 10 mg of tissue) supplemented with protein and protease inhibitors without detergents followed by incubation on ice for 45 min and centrifugation at +4°C for 20 min. Supernatants were collected and stored at -80°C until used for experiments. Protein concentration was determined via BCA assay (#23225, Thermo Fisher).

## 5.11 | RNA sequencing

RNA sequencing was performed at Novogene (Cambridge, UK). Prior to Illumina sequencing, the RNA underwent a thorough quality check and assessment for degradation via Agilent Bioanalyzer. The sequencing libraries were prepared with the NEBNext<sup>®</sup> UltraTM RNA Library Prep Kit (New England BioLabs, Ipswich). The libraries were sequenced using the Illumina HiSeq<sup>™</sup> 2000 platform.

## 5.12 | TMT-based quantitative mass spectrometry

Quantitative mass spectrometry (MS) analysis was performed on brain samples from three animals per group by the Proteomics Core Facility EMBL, Heidelberg, Germany. MS has been carried out independently for a specific project and consequently, the data will be published independently. Hence, solely GFAP data were selectively extracted for this particular objective.

Protein samples underwent isobaric labeling according to the manufacturer's instructions (TMT6plex Isobaric Label Reagent, ThermoFisher) before quantitative

LC–MS/MS via UltiMate 3000 RSLC nano-LC system (Dionex) as previously described (Dayon et al. 2008). The outlet of the analytical column was coupled directly to an Orbitrap Fusion™ Lumos™ Tribrid™ Mass Spectrometer (Thermo) using the Nanospray Flex™ ion source in positive ion mode. Full mass scan (MS1) was acquired with a mass range of 375–1500 m/z in profile mode in the orbitrap with a resolution of 60000. Data-dependent acquisition (DDA) was performed with the resolution of the Orbitrap set to 15000. The raw output files of IsobarQuant (protein.txt—files) were processed using the R programming language. Only proteins that were quantified with at least two unique peptides in at least two out of three replicates were considered for the analysis. Contra and Ipsi samples were treated separately. Proteins were tested for differential expression using the Limma R package. The FDR-adjusted *p*-values were then calculated separately using the fdrtool R package and the lower of the two *p*-values was selected. A protein was annotated as differentially expressed with a negative  $\log_{10}$  FDR-adjusted *p*-value greater than 1.301 (corresponding to an FDR-adjusted *p*-value <0.05).

### 5.13 | Brain immunochemistry control experiments

Considering we stained mouse brains with three primary antibodies, we carried out a series of control experiments to rigorously test for possible confounding effects stemming from the contemporary use of multiple primary antibodies:

#### A Testing for channel bleed-through

To probe for possible bleed-throughs between the microscopy channels used to visualize signals from three primary antibodies, respectively, we stained brain sections with all three primary antibodies and at the same time individually with each of the secondary antibodies and then analyzed spectral image lambda stacks to establish the emission spectra of each fluorophore and assess for possible spectral overlaps. The optimal image acquisition settings for the immunochemistry were defined based on careful assessment of the emission ranges during these control experiments, which showed no significant spectral overlap between the fluorophores.

#### B Testing for cross-reactivity of secondary antibodies

Applying the image acquisition settings defined based on the analysis of the spectral image lambda stacks, we imaged brain sections stained with all primary antibodies

and at the same time individually with each of the secondary antibodies to test for possible cross-reactivity of secondary with primary antibodies. Measurements of mean fluorescence of all individual secondary antibody conditions showed significant increase in mean fluorescence only with their corresponding and no other primary antibody.

#### C Testing cellular distributions of different fluorophore signals

The BIOP (Bioimaging and Optics Platform) version of JACop (Just Another Colocalisation Plugin) from the ImageJ was employed to analyze cellular distributions between different fluorophore signals, which could indirectly indicate the presence of possible channel bleed-through or secondary antibody cross-reactivity. Calculation of Pearson's coefficient was used to test for relationships between cellular distributions of different fluorophore signals.

### 5.14 | Sholl cell morphometric analysis

Cells included in the study were selected based on a systematic random selection based on the random number table. Moreover, only cells that showed clear nuclei and were fully recognizable were included in the study. Scholl analysis of astrocytes from the in vitro and in vivo studies was then performed via the Scholl plugin ImageJ as previously described.<sup>73</sup> In brief, Z-stack confocal images immunostained for GFAP were serially stacked and projected maximally. The maximal projection images of the GFAP signal in grayscale were adopted for the analysis. The plugging allowed drawing of serial concentric circles with 5- $\mu$ m intervals from the center of the soma to the end of the most distant process. The starting concentric radius started where the center of the cell soma ended for each sampled astrocyte. Intersections were determined as points where the astrocytic processes cross the concentric ring. The following parameters were selected for our study:

- Processes: number of processes originating directly from the cell soma.
- Sum of intersections: the total sum of crossings spotted on process sections.
- Mean intersections: the average number of intersections that occur across all the sampled radii covering astrocyte branches.
- Ramification index: the ratio between the maximum number of intersections and the number of processes.



- e. Enclosing radius: refers to the distance from the centre of a cell to the furthest outer region of the same cell.
- f. Number of intersections versus the distance from the soma: assesses the distribution of branching as a function of distance from the soma.

## 5.15 | Bioinformatics

Differential expression (DE) analysis of fragments per kilobase of transcript per million mapped reads (FPKM) normalized gene expression data was performed using the limma R package (with a linear model using weighted least squares, Empirical Bayes smoothing of standard errors, and moderated *t*-statistic with Benjamini–Hochberg *p*-values correction). DE analysis of the data presented in Figure 3I was performed using DESeq R package (with a model based on a negative binomial distribution and Benjamini and Hochberg *p*-values correction) for the genomics data and limma R package (with a linear model using weighted least squares, Empirical Bayes smoothing of standard errors, and moderated *t*-statistic with Benjamini–Hochberg *p*-values correction) for the proteomics data. A negative  $\log_{10}$  FDR adjusted *p*-value >1301 was set as the threshold for significant DE in all instances.

## 5.16 | Statistical analysis

Data are presented as mean  $\pm$  SEM. Differences between the two groups were analyzed using a *t*-test or mixed linear regression, depending on the nature of the data and the assumptions of each analysis. Multigroup differences were assessed by ANOVA, followed by a Tukey post hoc test for pairwise comparisons. All statistical analyses were performed as two-tailed, and a significance level of  $p < 0.05$  was considered statistically significant. Data analysis and visualizations were conducted using RStudio (version 2022.07.2 with R environment version 4.2.1) and GraphPad Prism 9 (La Jolla, USA).

## AUTHOR CONTRIBUTIONS

**Gretsen Velezmoro Jauregui:** Methodology; investigation; formal analysis; data curation; writing – review and editing; writing – original draft. **Dragana Vukić:** Methodology; investigation; formal analysis. **Isaac G. Onyango:** Methodology; investigation; formal analysis. **Carlos Arias:** Methodology; investigation. **Jan S. Novotný:** Formal analysis; data curation. **Kateřina Texlová:** Methodology; investigation. **Shanshan Wang:** Methodology; investigation. **Kristina Locker Kovačovicova:** Methodology; investigation; formal analysis. **Natalie Polakova:** Methodology; investigation.

**Jana Zelinkova:** Methodology; investigation. **Maria Čarna:** Methodology; investigation. **Valentina Lacovich:** Methodology; investigation. **Brian P. Head:** Methodology; investigation. **Daniel Havas:** Methodology; investigation; formal analysis; writing – review and editing. **Martin Mistrik:** Methodology; investigation. **Robert Zorec:** Methodology; writing – review and editing. **Alexei Verkhatsky:** Methodology; writing – original draft; writing – review and editing. **Liam Keegan:** Methodology; writing – review and editing. **Mary A. O'Connell:** Methodology; writing – review and editing. **Robert Rissman:** Methodology; writing – review and editing. **Gorazd B. Stokin:** Conceptualization; methodology; investigation; formal analysis; data curation; writing – original draft; writing – review and editing; supervision; project administration; funding acquisition.

## ACKNOWLEDGMENTS

We are most thankful for the continued feedback by Drs Clara Limbäck-Stokin and Kenneth Moya. We thank current and past members of the Stokin Lab for their support and feedback.

## FUNDING INFORMATION

The completion of this research project would not be possible without the support from the European Union: Next Generation EU—Project National Institute for Neurological Research (EXCELES, LX22NPO5107 (MEYS)) (G.B.S), the European Regional Development ENOCH grant CZ 02.1.01/0.0/16\_019/0000868 (G.B.S), the European Regional Development MAGNET grant CZ.02.1.01/0.0./15\_003/0000492 (G.B.S.), The Slovenian Research Agency project J3-50104 (R.Z.), the Slovenian Research Agency Core Research Program P3 310 Cell Physiology (R.Z.), the Interreg ITA-SLO ImmunoCluster-2; CipKeBip (R.Z), the Czech Science Foundation GAČR grant 21-27329X (M.A.O.C and LPK), the Czech Science Foundation GAČR 20-11101S (DV), the VA Merit Award (5I01BX003671) (B.P.H) and VA Research Career Scientist Award (1IK6BX006318) (B.P.H).

## CONFLICT OF INTEREST STATEMENT

The authors declare that they have no conflicts of interest regarding the publication of this manuscript. In the same line, this research was conducted in the absence of any commercial or financial relationships that could be construed as a potential conflict of interest.

## DATA AVAILABILITY STATEMENT

The authors confirm that the data supporting the findings of this study are available within the article and or its supplementary materials.

## ORCID

Gretsen Velezmoro Jauregui  <https://orcid.org/0000-0003-3176-3249>

Alexei Verkhratsky  <https://orcid.org/0000-0003-2592-9898>

Gorazd B. Stokin  <https://orcid.org/0000-0001-8430-8755>

## REFERENCES

- Semyanov A, Verkhratsky A. Astrocytic processes: from tripartite synapses to the active milieu. *Trends Neurosci.* 2021;44(10):781-792. doi:10.1016/j.tins.2021.07.006
- Araque A, Parpura V, Sanzgiri RP, Haydon PG. Tripartite synapses: glia, the unacknowledged partner. *Trends Neurosci.* 1999;22(5):208-215. doi:10.1016/s0166-2236(98)01349-6
- Augusto-Oliveira M. Astroglia-specific contributions to the regulation of synapses, cognition and behaviour. *Neurosci Biobehav Rev.* 2020;118:331-357. doi:10.1016/j.neubiorev.2020.07.039
- Durkee CA, Covelo A, Lines J, Kofuji P, Aguilar J, Araque A. G(i/o) protein-coupled receptors inhibit neurons but activate astrocytes and stimulate gliotransmission. *Glia.* 2019;67(6):1076-1093. doi:10.1002/glia.23589
- Südhof TC. Towards an understanding of synapse formation. *Neuron.* 2018;100(2):276-293. doi:10.1016/j.neuron.2018.09.040
- Andersen JaASaAV. Astrocyte energy and neurotransmitter metabolism in Alzheimer's disease: integration of the glutamate/GABA-glutamine cycle. *Prog Neurobiol.* 2022;217:102331. doi:10.1016/j.pneurobio.2022.102331
- Barros LF. How expensive is the astrocyte? *J Cereb Blood Flow Metab.* 2022;42(5):738-745. doi:10.1177/0271678x221077343
- Ghosh A, Cheung YY, Mansfield BC, Chou JY. Brain contains a functional glucose-6-phosphatase complex capable of endogenous glucose production. *J Biol Chem.* 2005;280(12):11114-11119. doi:10.1074/jbc.M410894200
- Subbarao KV, Hertz L. Effect of adrenergic agonists on glycolysis in primary cultures of astrocytes. *Brain Res.* 1990;536(1-2):220-226. doi:10.1016/0006-8993(90)90028-a
- Alvarez JJ, Katayama T, Prat A. Glial influence on the blood brain barrier. *Glia.* 2013;61(12):1939-1958. doi:10.1002/glia.22575
- Beck DW, Vinters HV, Hart MN, Cancilla PA. Glial cells influence polarity of the blood-brain barrier. *J Neuropathol Exp Neurol.* 1984;43(3):219-224. doi:10.1097/00005072-198405000-00001
- Verkhratsky A, Pivoriūnas A. Astroglia support, regulate and reinforce brain barriers. *Neurobiol Dis.* 2023;179:106054. doi:10.1016/j.nbd.2023.106054
- Vise WM, Liss L, Yashon D, Hunt WE. Astrocytic processes: a route between vessels and neurons following blood-brain barrier injury. *J Neuropathol Exp Neurol.* 1975;34(4):324-334. doi:10.1097/00005072-197507000-00002
- Escartin C, Galea E, Lakatos A, et al. Reactive astrocyte nomenclature, definitions, and future directions. *Nat Neurosci.* 2021;24(3):312-325. doi:10.1038/s41593-020-00783-4
- Verkhratsky A, Butt A, Li B, et al. Astrocytes in human central nervous system diseases: a frontier for new therapies. *Signal Transduct Target Ther.* 2023;8(1):396. doi:10.1038/s41392-023-01628-9
- Hol EM, Pekny M. Glial fibrillary acidic protein (GFAP) and the astrocyte intermediate filament system in diseases of the central nervous system. *Curr Opin Cell Biol.* 2015;32:121-130. doi:10.1016/j.ceb.2015.02.004
- Rodríguez JJ, Yeh CY, Terzieva S, Olabarria M, Kulijewicz-Nawrot M, Verkhratsky A. Complex and region-specific changes in astroglial markers in the aging brain. *Neurobiol Aging.* 2014;35(1):15-23. doi:10.1016/j.neurobiolaging.2013.07.002
- Pirnat S, Božić M, Dolanc D, et al. Astrocyte arborization enhances Ca(2+) but not cAMP signaling plasticity. *Glia.* 2021;69(12):2899-2916. doi:10.1002/glia.24076
- Leng K, Rose IVL, Kim H, et al. CRISPRi screens in human iPSC-derived astrocytes elucidate regulators of distinct inflammatory reactive states. *Nat Neurosci.* 2022;25(11):1528-1542. doi:10.1038/s41593-022-01180-9
- Liao MC, Muratore CR, Gierahn TM, et al. Single-cell detection of secreted Abeta and sAPPalpha from human iPSC-derived neurons and astrocytes. *J Neurosci.* 2016;36(5):1730-1746. doi:10.1523/JNEUROSCI.2735-15.2016
- Mathys H, Davila-Velderrain J, Peng Z, et al. Author correction: single-cell transcriptomic analysis of Alzheimer's disease. *Nature.* 2019;571(7763):E1. doi:10.1038/s41586-019-1329-6
- Todd BP, Chimenti MS, Luo Z, Ferguson PJ, Bassuk AG, Newell EA. Traumatic brain injury results in unique microglial and astrocyte transcriptomes enriched for type I interferon response. *J Neuroinflammation.* 2021;18(1):151. doi:10.1186/s12974-021-02197-w
- Zamanian JL, Xu L, Foo LC, et al. Genomic analysis of reactive astrogliosis. *J Neurosci.* 2012;32(18):6391-6410. doi:10.1523/JNEUROSCI.6221-11.2012
- Matejuk A, Ransohoff RM. Crosstalk between astrocytes and microglia: an overview. *Front Immunol.* 2020;11:1416. doi:10.3389/fimmu.2020.01416
- Thelin EP, Hall CE, Tyzack GE, et al. Delineating astrocytic cytokine responses in a human stem cell model of neural trauma. *J Neurotrauma.* 2020;37(1):93-105. doi:10.1089/neu.2019.6480
- Božić M, Verkhratsky A, Zorec R, Stenovec M. Exocytosis of large-diameter lysosomes mediates interferon  $\gamma$ -induced relocation of MHC class II molecules toward the surface of astrocytes. *Cell Mol Life Sci.* 2020;77(16):3245-3264. doi:10.1007/s00018-019-03350-8
- LeBlanc AC, Chen HY, Autilio-Gambetti L, Gambetti P. Differential APP gene expression in rat cerebral cortex, meninges, and primary astroglial, microglial and neuronal cultures. *FEBS Lett.* 1991;292(1-2):171-178. doi:10.1016/0014-5793(91)80861-v
- Martins RN, Taddei K, Kendall C, Evin G, Bates KA, Harvey AR. Altered expression of apolipoprotein E, amyloid precursor protein and presenilin-1 is associated with chronic reactive gliosis in rat cortical tissue. *Neuroscience.* 2001;106(3):557-569. doi:10.1016/s0306-4522(01)00289-5
- Müller UC, Deller T, Korte M. Not just amyloid: physiological functions of the amyloid precursor protein family. *Nat Rev Neurosci.* 2017;18(5):281-298. doi:10.1038/nrn.2017.29
- Müller UC, Zheng H. Physiological functions of APP family proteins. *Cold Spring Harb Perspect Med.* 2012;2(2):a006288. doi:10.1101/cshperspect.a006288
- Rohan de Silva HA, Jen A, Wickenden C, Jen LS, Wilkinson SL, Patel AJ. Cell-specific expression of beta-amyloid precursor protein isoform mRNAs and proteins in neurons and astrocytes.

- Brain Res Mol Brain Res.* 1997;47(1–2):147–156. doi:10.1016/S0169-328X(97)00045-4
32. Brugg B, Dubreuil YL, Huber G, Wollman EE, Delhaye-Bouchaud N, Mariani J. Inflammatory processes induce beta-amyloid precursor protein changes in mouse brain. *Proc Natl Acad Sci USA.* 1995;92(7):3032–3035. doi:10.1073/pnas.92.7.3032
  33. Hauss-Wegrzyniak B, Dobrzanski P, Stoehr JD, Wenk GL. Chronic neuroinflammation in rats reproduces components of the neurobiology of Alzheimer's disease. *Brain Res.* 1998;780(2):294–303. doi:10.1016/S0006-8993(97)01215-8
  34. Lee JW, Lee YK, Yuk DY, et al. Neuro-inflammation induced by lipopolysaccharide causes cognitive impairment through enhancement of beta-amyloid generation. *J Neuroinflammation.* 2008;5:37. doi:10.1186/1742-2094-5-37
  35. Kalehua AN, Taub DD, Baskar PV, et al. Aged mice exhibit greater mortality concomitant to increased brain and plasma TNF-alpha levels following intracerebroventricular injection of lipopolysaccharide. *Gerontology.* 2000;46(3):115–128. doi:10.1159/000022146
  36. Zhao J, O'Connor T, Vassar R. The contribution of activated astrocytes to A $\beta$  production: implications for Alzheimer's disease pathogenesis. *J Neuroinflammation.* 2011;8:150. doi:10.1186/1742-2094-8-150
  37. Blasko I, Veerhuis R, Stampfer-Kountchev M, Saurwein-Teissl M, Eikelenboom P, Grubeck-Loebenstein B. Costimulatory effects of interferon-gamma and interleukin-1beta or tumor necrosis factor alpha on the synthesis of Abeta1-40 and Abeta1-42 by human astrocytes. *Neurobiol Dis.* 2000;7(6 Pt B):682–689. doi:10.1006/nbdi.2000.0321
  38. Gray CW, Patel AJ. Induction of beta-amyloid precursor protein isoform mRNAs by bFGF in astrocytes. *Neuroreport.* 1993;4(6):811–814. doi:10.1097/00001756-199306000-00054
  39. Gray CW, Patel AJ. Regulation of beta-amyloid precursor protein isoform mRNAs by transforming growth factor-beta 1 and interleukin-1 beta in astrocytes. *Brain Res Mol Brain Res.* 1993;19(3):251–256. doi:10.1016/0169-328X(93)90037-p
  40. Sheng JG, Bora SH, Xu G, Borchelt DR, Price DL, Koliatsos VE. Lipopolysaccharide-induced-neuroinflammation increases intracellular accumulation of amyloid precursor protein and amyloid beta peptide in APP<sup>swe</sup> transgenic mice. *Neurobiol Dis.* 2003;14(1):133–145. doi:10.1016/S0969-9961(03)00069-x
  41. Burton T, Liang B, Dibrov A, Amara F. Transforming growth factor-beta-induced transcription of the Alzheimer beta-amyloid precursor protein gene involves interaction between the CTCF-complex and Smads. *Biochem Biophys Res Commun.* 2002;295(3):713–723. doi:10.1016/S0006-291X(02)00725-8
  42. Palacios G, Mengod G, Tortosa A, Ferrer I, Palacios JM. Increased beta-amyloid precursor protein expression in astrocytes in the gerbil hippocampus following ischaemia: association with proliferation of astrocytes. *Eur J Neurosci.* 1995;7(3):501–510. doi:10.1111/j.1460-9568.1995.tb00346.x
  43. Otsuka N, Tomonaga M, Ikeda K. Rapid appearance of beta-amyloid precursor protein immunoreactivity in damaged axons and reactive glial cells in rat brain following needle stab injury. *Brain Res.* 1991;568(1–2):335–338. doi:10.1016/0006-8993(91)91422-w
  44. Siman R, Card JP, Nelson RB, Davis LG. Expression of beta-amyloid precursor protein in reactive astrocytes following neuronal damage. *Neuron.* 1989;3(3):275–285. doi:10.1016/0896-6273(89)90252-3
  45. Shepherd CE, Bowes S, Parkinson D, Cambrey-Deakin M, Pearson RC. Expression of amyloid precursor protein in human astrocytes in vitro: isoform-specific increases following heat shock. *Neuroscience.* 2000;99(2):317–325. doi:10.1016/S0306-4522(00)00197-4
  46. Clarner T, Buschmann JP, Beyer C, Kipp M. Glial amyloid precursor protein expression is restricted to astrocytes in an experimental toxic model of multiple sclerosis. *J Mol Neurosci.* 2011;43(3):268–274. doi:10.1007/s12031-010-9419-9
  47. Töpfer R, Gehrmann J, Banati R, et al. Rapid appearance of beta-amyloid precursor protein immunoreactivity in glial cells following excitotoxic brain injury. *Acta Neuropathol.* 1995;89(1):23–28. doi:10.1007/bf00294255
  48. Komatsu A, Iida I, Nasu Y, et al. Ammonia induces amyloidogenesis in astrocytes by promoting amyloid precursor protein translocation into the endoplasmic reticulum. *J Biol Chem.* 2022;298(5):101933. doi:10.1016/j.jbc.2022.101933
  49. Delarasse C, Auger R, Gonnord P, Fontaine B, Kanellopoulos JM. The purinergic receptor P2X7 triggers alpha-secretase-dependent processing of the amyloid precursor protein. *J Biol Chem.* 2011;286(4):2596–2606. doi:10.1074/jbc.M110.200618
  50. Lee RK, Araki W, Wurtman RJ. Stimulation of amyloid precursor protein synthesis by adrenergic receptors coupled to cAMP formation. *Proc Natl Acad Sci USA.* 1997;94(10):5422–5426. doi:10.1073/pnas.94.10.5422
  51. Fontana A, Weber E, Grob PJ, Lim R, Miller JF. Dual effect of glia maturation factor on astrocytes. Differentiation and release of interleukin-1 like factors. *J Neuroimmunol.* 1983;5(3):261–269. doi:10.1016/0165-5728(83)90046-2
  52. Frei K, Bodmer S, Schwerdel C, Fontana A. Astrocyte-derived interleukin 3 as a growth factor for microglia cells and peritoneal macrophages. *J Immunol.* 1986;137(11):3521–3527.
  53. Griffin WS, Stanley LC, Ling C, et al. Brain interleukin 1 and S-100 immunoreactivity are elevated in Down syndrome and Alzheimer disease. *Proc Natl Acad Sci USA.* 1989;86(19):7611–7615. doi:10.1073/pnas.86.19.7611
  54. Liang Y, Raven F, Ward JF, et al. Upregulation of Alzheimer's disease amyloid- $\beta$  protein precursor in astrocytes both in vitro and in vivo. *J Alzheimers Dis.* 2020;76(3):1071–1082. doi:10.3233/jad-200128
  55. Motwani M, Pesiridis S, Fitzgerald KA. DNA sensing by the cGAS-STING pathway in health and disease. *Nat Rev Genet.* 2019;20(11):657–674. doi:10.1038/s41576-019-0151-1
  56. Eckman CB, Mehta ND, Crook R, et al. A new pathogenic mutation in the APP gene (I716V) increases the relative proportion of A beta 42(43). *Hum Mol Genet.* 1997;6(12):2087–2089. doi:10.1093/hmg/6.12.2087
  57. Kamino K, Orr HT, Payami H, et al. Linkage and mutational analysis of familial Alzheimer disease kindreds for the APP gene region. *Am J Hum Genet.* 1992;51(5):998–1014.
  58. Kumar-Singh S, De Jonghe C, Cruts M, et al. Nonfibrillar diffuse amyloid deposition due to a gamma(42)-secretase site mutation points to an essential role for N-truncated A beta(42) in Alzheimer's disease. *Hum Mol Genet.* 2000;9(18):2589–2598. doi:10.1093/hmg/9.18.2589
  59. Mullan M, Crawford F, Axelman K, et al. A pathogenic mutation for probable Alzheimer's disease in the APP gene at the



- N-terminus of beta-amyloid. *Nat Genet.* 1992;1(5):345-347. doi:10.1038/ng0892-345
60. Peacock ML, Warren JT Jr, Roses AD, Fink JK. Novel polymorphism in the A4 region of the amyloid precursor protein gene in a patient without Alzheimer's disease. *Neurology.* 1993;43(6):1254-1256. doi:10.1212/wnl.43.6.1254
  61. Niesman IR, Schilling JM, Shapiro LA, et al. Traumatic brain injury enhances neuroinflammation and lesion volume in caveolin deficient mice. *J Neuroinflammation.* 2014;11:39. doi:10.1186/1742-2094-11-39
  62. Myer DJ, Gurkoff GG, Lee SM, Hovda DA, Sofroniew MV. Essential protective roles of reactive astrocytes in traumatic brain injury. *Brain.* 2006;129(Pt 10):2761-2772. doi:10.1093/brain/awl165
  63. Rogers JT, Leiter LM, McPhee J, et al. Translation of the alzheimer amyloid precursor protein mRNA is up-regulated by interleukin-1 through 5'-untranslated region sequences. *J Biol Chem.* 1999;274(10):6421-6431. doi:10.1074/jbc.274.10.6421
  64. Cieri MB, Villarreal A, Gomez-Cuautle DD, Mailing I, Ramos AJ. Progression of reactive gliosis and astroglial phenotypic changes following stab wound-induced traumatic brain injury in mice. *J Neurochem.* 2023;167(2):183-203. doi:10.1111/jnc.15941
  65. Lau LT, Yu AC. Astrocytes produce and release interleukin-1, interleukin-6, tumor necrosis factor alpha and interferon-gamma following traumatic and metabolic injury. *J Neurotrauma.* 2001;18(3):351-359. doi:10.1089/08977150151071035
  66. Liu Y, Hong W, Gong P, et al. Specific knockout of Sox2 in astrocytes reduces reactive astrocyte formation and promotes recovery after early postnatal traumatic brain injury in mouse cortex. *Glia.* 2023;71(3):602-615. doi:10.1002/glia.24298
  67. Wangler LM, Bray CE, Packer JM, et al. Amplified gliosis and interferon-associated inflammation in the aging brain following diffuse traumatic brain injury. *J Neurosci.* 2022;42(48):9082-9096. doi:10.1523/jneurosci.1377-22.2022
  68. Preman P, Alfonso-Triguero M, Alberdi E, Verkhratsky A, Arranz AM. Astrocytes in Alzheimer's disease: pathological significance and molecular pathways. *Cells.* 2021;10(3):540. doi:10.3390/cells10030540
  69. Preman P, Tew J, Calafate S, et al. Human iPSC-derived astrocytes transplanted into the mouse brain undergo morphological changes in response to amyloid- $\beta$  plaques. *Mol Neurodegener.* 2021;16(1):68. doi:10.1186/s13024-021-00487-8
  70. Sanalkumar R, Vidyanand S, Lalitha Indulekha C, James J. Neuronal vs. glial fate of embryonic stem cell-derived neural progenitors (ES-NPs) is determined by FGF2/EGF during proliferation. *J Mol Neurosci.* 2010;42(1):17-27. doi:10.1007/s12031-010-9335-z
  71. Abu Hamdeh S, Shevchenko G, Mi J, Musunuri S, Bergquist J, Marklund N. Proteomic differences between focal and diffuse traumatic brain injury in human brain tissue. *Sci Rep.* 2018;8(1):6807. doi:10.1038/s41598-018-25060-0
  72. Dozio V, Sanchez JC. Profiling the proteomic inflammatory state of human astrocytes using DIA mass spectrometry. *J Neuroinflammation.* 2018;15(1):331. doi:10.1186/s12974-018-1371-6
  73. Sholl DA. Dendritic organization in the neurons of the visual and motor cortices of the cat. *J Anat.* 1953;87(4):387-406. September 2023. <https://www.ncbi.nlm.nih.gov/pubmed/13117757>
  74. Busciglio J, Gabuzda DH, Matsudaira P, Yankner BA. Generation of beta-amyloid in the secretory pathway in neuronal and non-neuronal cells. *Proc Natl Acad Sci USA.* 1993;90(5):2092-2096. doi:10.1073/pnas.90.5.2092
  75. Forman MS, Cook DG, Leight S, Doms RW, Lee VM. Differential effects of the swedish mutant amyloid precursor protein on beta-amyloid accumulation and secretion in neurons and nonneuronal cells. *J Biol Chem.* 1997;272(51):32247-32253. doi:10.1074/jbc.272.51.32247
  76. Haass C, Hung AY, Selkoe DJ. Processing of beta-amyloid precursor protein in microglia and astrocytes favors an internal localization over constitutive secretion. *J Neurosci.* 1991;11(12):3783-3793. doi:10.1523/jneurosci.11-12-03783.1991
  77. LeBlanc AC, Xue R, Gambetti P. Amyloid precursor protein metabolism in primary cell cultures of neurons, astrocytes, and microglia. *J Neurochem.* 1996;66(6):2300-2310. doi:10.1046/j.1471-4159.1996.66062300.x
  78. Peppercorn K, Kleffmann T, Hughes SM, Tate WP. Secreted amyloid precursor protein alpha (sAPP $\alpha$ ) regulates the cellular proteome and secretome of mouse primary astrocytes. *Int J Mol Sci.* 2023;24(8). doi:10.3390/ijms24087165
  79. Mönning U, König G, Banati RB, et al. Alzheimer beta A4-amyloid protein precursor in immunocompetent cells. *J Biol Chem.* 1992;267(33):23950-23956.
  80. Solà C, García-Ladona FJ, Mengod G, Probst A, Frey P, Palacios JM. Increased levels of the Kunitz protease inhibitor-containing beta APP mRNAs in rat brain following neurotoxic damage. *Brain Res Mol Brain Res.* 1993;17(1-2):41-52. doi:10.1016/0169-328x(93)90071-v
  81. Young MJ, Lee RK, Jhaveri S, Wurtman RJ. Intracellular and cell-surface distribution of amyloid precursor protein in cortical astrocytes. *Brain Res Bull.* 1999;50(1):27-32. doi:10.1016/s0361-9230(99)00084-2
  82. Neve RL, Finch EA, Dawes LR. Expression of the Alzheimer amyloid precursor gene transcripts in the human brain. *Neuron.* 1988;1(8):669-677. doi:10.1016/0896-6273(88)90166-3
  83. Tanaka S, Nakamura S, Ueda K, et al. Three types of amyloid protein precursor mRNA in human brain: their differential expression in Alzheimer's disease. *Biochem Biophys Res Commun.* 1988;157(2):472-479. doi:10.1016/s0006-291x(88)80273-0
  84. Hu J, Akama KT, Krafft GA, Chromy BA, Van Eldik LJ. Amyloid-beta peptide activates cultured astrocytes: morphological alterations, cytokine induction and nitric oxide release. *Brain Res.* 1998;785(2):195-206. doi:10.1016/s0006-8993(97)01318-8
  85. Johnstone M, Gearing AJ, Miller KM. A central role for astrocytes in the inflammatory response to beta-amyloid; chemokines, cytokines and reactive oxygen species are produced. *J Neuroimmunol.* 1999;93(1-2):182-193. doi:10.1016/s0165-5728(98)00226-4
  86. LaRocca TJ, Cavalier AN, Roberts CM, et al. Amyloid beta acts synergistically as a pro-inflammatory cytokine. *Neurobiol Dis.* 2021;159:105493. doi:10.1016/j.nbd.2021.105493
  87. Leng F, Hinz R, Gentleman S, et al. Neuroinflammation is independently associated with brain network dysfunction in Alzheimer's disease. *Mol Psychiatry.* 2023;28(3):1303-1311. doi:10.1038/s41380-022-01878-z
  88. Kulijewicz-Nawrot M, Verkhratsky A, Chvátal A, Syková E, Rodríguez JJ. Astrocytic cytoskeletal atrophy in the medial prefrontal cortex of a triple transgenic mouse model



- of Alzheimer's disease. *J Anat.* 2012;221(3):252-262. doi:[10.1111/j.1469-7580.2012.01536.x](https://doi.org/10.1111/j.1469-7580.2012.01536.x)
89. Yeh CY, Vadhvana B, Verkhatsky A, Rodríguez JJ. Early astrocytic atrophy in the entorhinal cortex of a triple transgenic animal model of Alzheimer's disease. *ASN Neuro.* 2011;3(5):271-279. doi:[10.1042/an20110025](https://doi.org/10.1042/an20110025)
  90. de Rivero Vaccari JP, Brand FJ 3rd, Sedaghat C, Mash DC, Dietrich WD, Keane RW. RIG-I receptor expression in the pathology of Alzheimer's disease. *J Neuroinflammation.* 2014;11:67. doi:[10.1186/1742-2094-11-67](https://doi.org/10.1186/1742-2094-11-67)
  91. Hur JY, Frost GR, Wu X, et al. The innate immunity protein IFITM3 modulates  $\gamma$ -secretase in Alzheimer's disease. *Nature.* 2020;586(7831):735-740. doi:[10.1038/s41586-020-2681-2](https://doi.org/10.1038/s41586-020-2681-2)
  92. Hunter S, Brayne C. Relationships between the amyloid precursor protein and its various proteolytic fragments and neuronal systems. *Alzheimers Res Ther.* 2012;4(2):10. doi:[10.1186/alzrt108](https://doi.org/10.1186/alzrt108)
  93. Webers A, Heneka MT, Gleeson PA. The role of innate immune responses and neuroinflammation in amyloid accumulation and progression of Alzheimer's disease. *Immunol Cell Biol.* 2020;98(1):28-41. doi:[10.1111/imcb.12301](https://doi.org/10.1111/imcb.12301)
  94. Barish ME, Mansdorf NB, Raissdana SS. Gamma-interferon promotes differentiation of cultured cortical and hippocampal neurons. *Dev Biol.* 1991;144(2):412-423. doi:[10.1016/0012-1606\(91\)90433-4](https://doi.org/10.1016/0012-1606(91)90433-4)
  95. Bourgeade MF, Rousset S, Paulin D, Chany C. Reorganization of the cytoskeleton by interferon in MSV-transformed cells. *J Interf Res.* 1981;1(2):323-332. doi:[10.1089/jir.1981.1.323](https://doi.org/10.1089/jir.1981.1.323)
  96. Hashioka S, McGeer EG, Miyaoka T, Wake R, Horiguchi J, McGeer PL. Interferon- $\gamma$ -induced neurotoxicity of human astrocytes. *CNS Neurol Disord Drug Targets.* 2015;14(2):251-256. doi:[10.2174/1871527314666150217122305](https://doi.org/10.2174/1871527314666150217122305)
  97. Hovi T, Lehto VP, Virtanen I. Interferon affects the formation of adhesion plaques in human monocyte cultures. *Exp Cell Res.* 1985;159(2):305-312. doi:[10.1016/s0014-4827\(85\)80004-5](https://doi.org/10.1016/s0014-4827(85)80004-5)
  98. Plioplys AV. Expression of the 210 kDa neurofilament subunit in cultured central nervous system from normal and trisomy 16 mice: regulation by interferon. *J Neurol Sci.* 1988;85(2):209-222. doi:[10.1016/0022-510x\(88\)90157-8](https://doi.org/10.1016/0022-510x(88)90157-8)
  99. Ulker N, Zhang X, Samuel CE. Mechanism of interferon action. I. Characterization of a 54-kDa protein induced by gamma interferon with properties similar to a cytoskeletal component. *J Biol Chem.* 1987;262(35):16798-16803.
  100. Eckfeld C, Schoeps B, Häußler D, et al. TIMP-1 is a novel ligand of amyloid precursor protein and triggers a proinflammatory phenotype in human monocytes. *J Cell Biol.* 2023;222(2):e202206095. doi:[10.1083/jcb.202206095](https://doi.org/10.1083/jcb.202206095)
  101. Sondag CM, Combs CK. Amyloid precursor protein mediates proinflammatory activation of monocytic lineage cells. *J Biol Chem.* 2004;279(14):14456-14463. doi:[10.1074/jbc.M313747200](https://doi.org/10.1074/jbc.M313747200)
  102. Sondag CM, Combs CK. Amyloid precursor protein cross-linking stimulates beta amyloid production and pro-inflammatory cytokine release in monocytic lineage cells. *J Neurochem.* 2006;97(2):449-461. doi:[10.1111/j.1471-4159.2006.03759.x](https://doi.org/10.1111/j.1471-4159.2006.03759.x)
  103. Sondag CM, Combs CK. Adhesion of monocytes to type I collagen stimulates an APP-dependent proinflammatory signaling response and release of Abeta1-40. *J Neuroinflammation.* 2010;7:22. doi:[10.1186/1742-2094-7-22](https://doi.org/10.1186/1742-2094-7-22)
  104. Carrano A, Das P. Altered innate immune and glial cell responses to inflammatory stimuli in amyloid precursor protein knockout mice. *PLoS One.* 2015;10(10):e0140210. doi:[10.1371/journal.pone.0140210](https://doi.org/10.1371/journal.pone.0140210)
  105. Sanford SAI, Miller LVC, Vaysburd M, et al. The type-I interferon response potentiates seeded tau aggregation and exacerbates tau pathology. *Alzheimers Dement.* 2023;19:1013-1025. doi:[10.1002/alz.13493](https://doi.org/10.1002/alz.13493)
  106. Boghdadi AG, Teo L, Bourne JA. The neuroprotective role of reactive astrocytes after central nervous system injury. *J Neurotrauma.* 2020;37(5):681-691. doi:[10.1089/neu.2019.6938](https://doi.org/10.1089/neu.2019.6938)
  107. O'Shea TM, Ao Y, Wang S, et al. Border-forming wound repair astrocytes. *bioRxiv.* 2023. doi:[10.1101/2023.08.25.554857](https://doi.org/10.1101/2023.08.25.554857)
  108. Plummer S, Van den Heuvel C, Thornton E, Corrigan F, Cappai R. The neuroprotective properties of the amyloid precursor protein following traumatic brain injury. *Aging Dis.* 2016;7(2):163-179. doi:[10.14336/ad.2015.0907](https://doi.org/10.14336/ad.2015.0907)
  109. Luu L, Ciccotosto GD, Cappai R. The Alzheimer's disease amyloid precursor protein and its neuritogenic actions. *Curr Alzheimer Res.* 2021;18(10):772-786. doi:[10.2174/156720501866211208141017](https://doi.org/10.2174/156720501866211208141017)
  110. Arai N. The role of swollen astrocytes in human brain lesions after edema—an immunohistochemical study using formalin-fixed paraffin-embedded sections. *Neurosci Lett.* 1992;138(1):56-58. doi:[10.1016/0304-3940\(92\)90471-i](https://doi.org/10.1016/0304-3940(92)90471-i)
  111. Brenner M, Johnson AB, Boespflug-Tanguy O, Rodriguez D, Goldman JE, Messing A. Mutations in GFAP, encoding glial fibrillary acidic protein, are associated with Alexander disease. *Nat Genet.* 2001;27(1):117-120. doi:[10.1038/83679](https://doi.org/10.1038/83679)
  112. De Groot CJ, Montagne L, Barten AD, Sminia P, Van Der Valk P. Expression of transforming growth factor (TGF)-beta1, -beta2, and -beta3 isoforms and TGF-beta type I and type II receptors in multiple sclerosis lesions and human adult astrocyte cultures. *J Neuropathol Exp Neurol.* 1999;58(2):174-187. doi:[10.1097/00005072-199902000-00007](https://doi.org/10.1097/00005072-199902000-00007)
  113. Zheng H, Jiang M, Trumbauer ME, et al. beta-Amyloid precursor protein-deficient mice show reactive gliosis and decreased locomotor activity. *Cell.* 1995;81(4):525-531. doi:[10.1016/0092-8674\(95\)90073-x](https://doi.org/10.1016/0092-8674(95)90073-x)
  114. Schneider CA, Rasband WS, Eliceiri KW. NIH Image to ImageJ: 25 years of image analysis. *Nat Methods.* 2012;9(7):671-675. doi:[10.1038/nmeth.2089](https://doi.org/10.1038/nmeth.2089)

## SUPPORTING INFORMATION

Additional supporting information can be found online in the Supporting Information section at the end of this article.

**How to cite this article:** Velezmoro Jauregui G, Vukić D, Onyango IG, et al. Amyloid precursor protein induces reactive astrogliosis. *Acta Physiol.* 2024;00:e14142. doi:[10.1111/apha.14142](https://doi.org/10.1111/apha.14142)